Otterbein University

Digital Commons @ Otterbein

Spring 2015

Analysis of the Energy Spectrum of Michel Electrons In MicroBooNE

Philip Griffith Kellogg
Otterbein University, philip.kellogg@otterbein.edu

Follow this and additional works at: https://digitalcommons.otterbein.edu/stu_honor

Part of the Elementary Particles and Fields and String Theory Commons

Recommended Citation

Kellogg, Philip Griffith, "Analysis of the Energy Spectrum of Michel Electrons In MicroBooNE" (2015). *Undergraduate Honors Thesis Projects*. 15.
https://digitalcommons.otterbein.edu/stu_honor/15

ANALYSIS OF THE ENERGY SPECTRUM OF MICHEL ELECTRONS IN
MICROBOONE

by

Philip Griffith Kellogg
Department of Physics
Otterbein University
Westerville, Ohio 43081

April 2, 2015

Submitted in partial fulfillment of the requirements
For graduation with Honors

<u>Dr. Nathaniel Tagg, PhD.</u>   _____
Honors Advisor   Advisor's Signature

<u>Dr. Aaron Reinhard, Ph.D.</u>   _____
Second Reader   Second Reader's Signature

<u>Dr. Wendy Sherman Heckler, Ph.D.</u>   _____
Honors Representative   Honors Rep's Signature

i. Acknowledgements

I would like to thank Dr. Nathaniel Tagg for his much needed guidance and patience with me and this project. It would not have been possible without his help. I would like to thank Dr. Aaron Reinhard for taking the time to be my second reader and help me better explain the content to my project. I would also like a acknowledge the National Science foundation and Fermi National accelerator Laboratory for funding and hosting MicroBooNE, around which my work is based.

ii. Abstract

The MicroBooNE experiment at Fermilab was designed both to investigate results from anomalies seen in short-baseline experiments and to prototype technology for larger scale experiments. MicroBooNE hopes to investigate an excess of low-energy events seen in a preceding experiment, using improved detector resolution. The goal of this thesis was to perform a calibration of the MicroBooNE detector by determining the Michel electron energy spectrum inside the detector. Michel electrons result from the decay of muons, and have a very well understood energy spectrum. Muons from cosmic rays continually pass through the detector, roughly 1% of which will decay within the detector volume. From these decayed muons it is possible to measure the energy spectrum of Michel decays occurring within the detector. Comparison of this spectrum with the spectrum provided by theory gives a conversion factor between the arbitrary detector units and true energy in MeV. This calibration is necessary for producing good physics data to meet the goals of the experiment. Here a procedure is developed that performs robust, low-level calibration. Development started with a simplified scenario, and ended with a more high-level calibration procedure, which found the detector to be calibrated at 54 ± 8 ADC/MeV.

iii. Table of Contents   **Page**

iv. List of Figures   **Page**

1. Introduction

The concept behind this project was to find a way to calibrate a liquid argon detector, specifically the detector for the Micro Booster Neutrino Experiment (MicroBooNE) at Fermi National Accelerator Laboratory (Fermilab).The goal was to perform a calibration of the detector. However the method by which the detector was calibrated was designed to easily translate into an automated process to continuously run over data from the experiment, as it became available, in order to perform a continuous low-level check of the detector's functionality. In other words, to ensure that as the experiment continues there is no significant shift in the calibration factor for the detector.

1.1 Neutrinos and Oscillation

Fermilab, located just outside of Chicago in Batavia, Illinois, is one of the largest physics research laboratories in the nation, and is funded by the Department of Energy. Much of the current physics under investigation at Fermilab is focused on small, weakly interacting, elementary particles known as neutrinos. Neutrinos comprise three of the known elementary particles of the standard model, each flavor corresponding with another lepton: electron neutrinos with electrons; muon neutrinos with muons; tau neutrinos with tauons.

Neutrinos were first proposed in 1930 by Wolfgang Pauli, as an explanation for discrepancies seen in beta decay. In beta decay one of an atom's neutrons converts into a proton, which remains bound to the nucleus, and an electron, which is emitted from the atom. However, the new atom and released electron appeared to violate conservation of momentum, energy, and particle spin. Rather than discount these fundamental physical

principles, Pauli suggested the presence of an as-yet undiscovered particle, which was neutral and weakly interacting. However, the presence of the this particle was not experimentally confirmed until 1956. After the discovery of this neutrino, which is now known as the muon neutrino, the other flavors of neutrinos, corresponding to the other known leptons, were discovered.

As the study of neutrinos continued, it was found that they possessed a unique property known as oscillation. As neutrinos travel they oscillate between flavors. Many experiments were designed to investigate this property, including several at Fermilab. One of these experiments, MiniBooNE (a precursor to MicroBooNE) measured a significant excess of low energy events while studying $v_\mu \rightarrow v_e$ oscillations, see Fig. 1. (7) However, due to the resolution limits of MiniBooNE, it is unknown whether the excess was the result of electron or photon producing interactions. An excess due to photons is thought to imply that the theoretical model used to determine the expected results of the experiments was incorrect. The largest portion of the background in the detector is due decays unrelated to neutrino oscillations, which result in photons. However, if the excess was the result of electron-like events theoretical models have suggested the excess might be due to an oscillation involving a fourth flavor of neutrino, known as a sterile neutrino. (7) Given this possibility, a new style of detector was needed that could run in the same configuration as MiniBooNE and using the same beam source, but with the ability to discriminate electron and photon-like events.
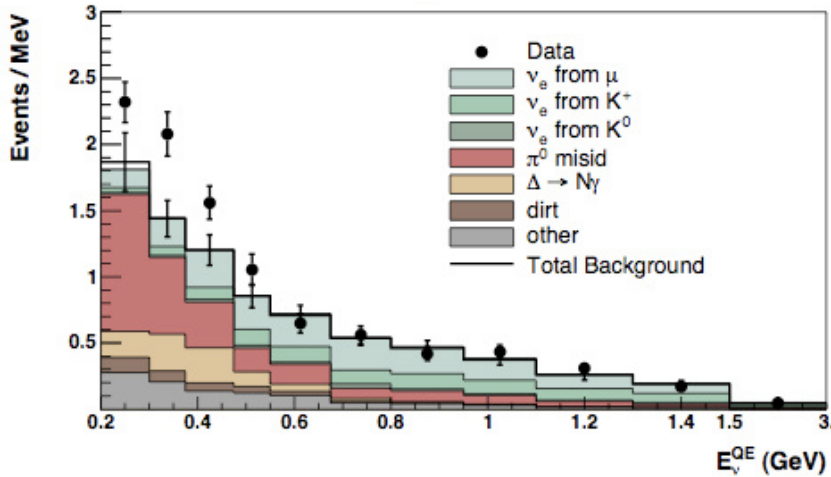
Figure 1: This plot shows distribution of events expected for MiniBooNE by source in a stacked histogram. At low energy, the experimentally measured number of events (Data) is significantly larger than theory. However, theory and experiment agree at high energies. (7)

1.2 The Booster Beam

The Booster Beam is one of the neutrino beams used by experiments at Fermilab. The first step in creating the Booster Neutrino Beam (BNB) involves bringing roughly 10^{12} protons up to 8 GeV of kinetic energy using a circular accelerator, known as the Booster Ring. (8) These protons are then fired at a graphite target, creating a shower of particles, with the product of interest being pions. Pions from this shower are sent through a magnetic horn, which focuses the beam. This beam of pions is then sent through a long pipe, where they naturally decay into muons and muon neutrinos. At the end of the pipe is a large brick wall, which stops the muons, while the neutrinos pass straight through, leaving a purely neutrino beam. Experiments, such as MicroBooNE, can then be lined up along the path of the beam in order to observe neutrino events.

Neutrinos interact only via the weak interaction, meaning they very rarely interact.(1) Even with the large number of protons on target from the BNB, which produces the same order number of neutrinos per pulse , and the beam at roughly ~5 Hz, a detector will only see 1-20 events per day.(7,8) Any number of detectors can be lined

up along a given beam without limiting the statistics of any experiments downstream. In fact the only factor that has a large effect on beam intensity is the natural beam spread which occurs as you get further downstream from the beam. On site the beam width is such that it is spread evenly across the detector.

1.3 MicroBooNE

MicroBooNE, the Micro Booster Neutrino Experiment, was designed with three goals in mind. The first is to test the low-energy excess seen in MiniBooNE, by running in the same Booster Beam configuration as MiniBooNE, and using a different detection medium (liquid argon rather than oil), but with improved technologies for detector resolution. The second goal is to measure neutrino differential cross-sections in liquid argon. The third goal is to act as a stepping stone and large scale model to an even larger experiment that will be based off the same detector design: the Long-Baseline Neutrino Experiment (LBNE). (4,7) The new detector technologies being tested in MicroBooNE will significantly enhance event reconstruction and readout in order to the improve understanding of the physics of neutrino interactions and oscillations. (7)

The MicroBooNE detector is composed of a large metal cage, sealed in a hundred-ton scale, cylindrical cryostat, filled with liquid argon. The cage is approximately 10 meters long, with a 2.3m by 2.6 m rectangular cross-section, see Fig 2. The entire detector is housed in a dedicated building on-site at Fermilab, known as the Liquid Argon Test Facility (LArTF) which extends six stories below ground so that the detector can align with the Booster Beam, see Fig. 3. (7)

The detector cage is composed of metal tubes circling the detector, oriented down its length, and spaced from beam-left to right, see Fig. 2. These bars are each held at a potential 2kV higher than the preceding tube, going from the beam-left to the beam-right side of the detector. This establishes a uniform 500 V/cm field, oriented from the beam-right side of the detector cage to the beam-left, see Fig. 4. Electrons resulting from the ionization of the liquid argon by particles passing through the detector will be drifted by the field to the beam-right side of the cage (positive X, as seen in Fig. 4), where the readout electronics are held.
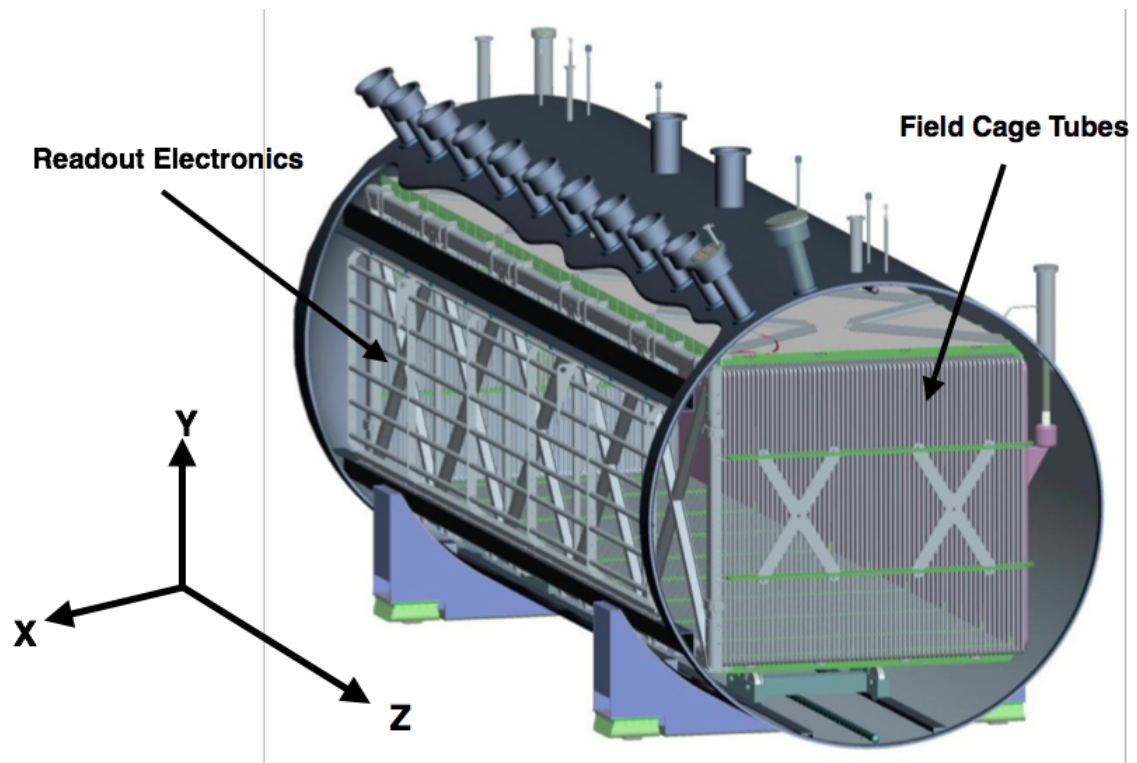
Fig. 2: The MicroBooNE detector, oriented such that the beam would be coming out of the page in the Z direction. The readout electronics on the left side of the image, include the three planes of wires and an array of PMTs, with channels running out the tubes on the top of the cryostat. The field cage tubes, which wrap around the detector and run parallel to the YZ plane, establish a field across the detector cage, oriented in the negative X direction, to drift electrons to the readout electronics. (7)
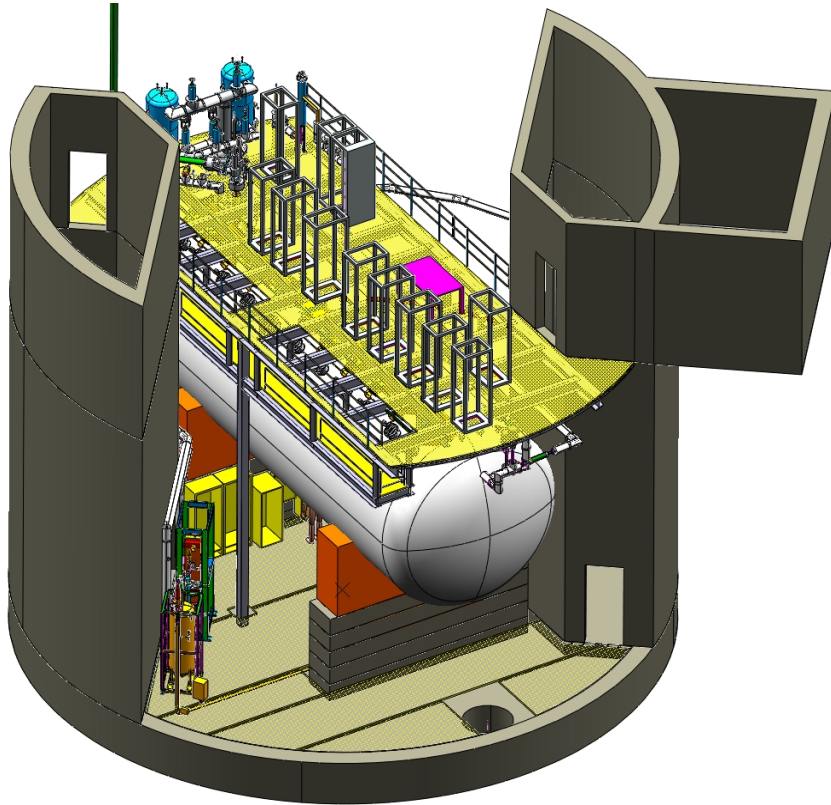
Fig 3: The detector fully insulated in the cryostat (white in the image) housed in LArTF. The warm electronics and data storage are housed on racks above the detector (yellow). The doorways in the bottom left and top right provide a sense of scale. (7)

Fig 4: An overhead cross sectional view of the detector, oriented such that the beam will pass from left to right, Z. The field cage establishes an electric field across the detector cage, oriented from beam-left (top) to beam-right (bottom), -X, such that ionization electrons drift to the readout wires (bottom).

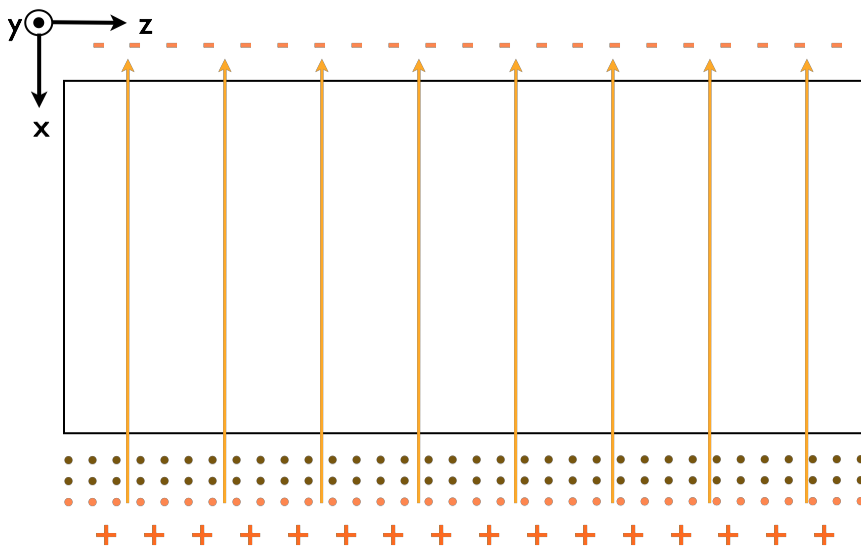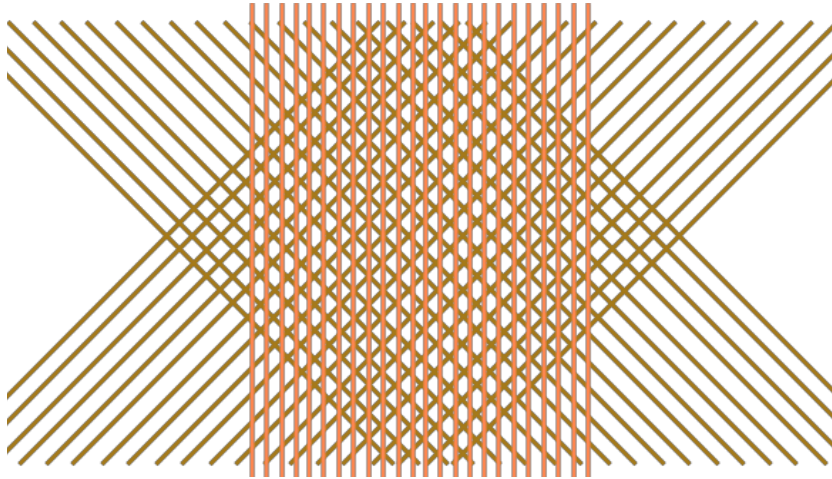**Fig 5:**Orientation of the induction and collection wires, as viewed from the outside of the beam-right side of the detector. The two induction planes, known as the U and V planes, are each offset 60º, from the horizontal, while the collection plane is oriented vertically.

The beam-right side of the detector cage is lined with three planes of wires, with 3mm spacing. Observing the cage along the direction of the beam, the first two layers of wires are oriented on a diagonal such that one is 60 degrees displaced from the vertical towards the front of the detector, and one is displaced 60 degrees from the vertical in the opposite direction, towards the far end of the detector. These two planes of wires are known as the induction planes. Behind these two planes is a third plane known as the collection plane, which is oriented with the vertical, see Fig. 5.

When neutrinos enter the detector they can only be detected by observation of a single interaction. Unlike the majority of the particles produced by these interactions, neutrinos are close to massless, and interact only via the weak interaction(1). Though the beam results from 5×10^{12} protons per-pulse, which produces a similar order of neutrinos, and beam pulses arrive at a rate of ~5 Hz, only a few of events are seen in the detector each per day(7). When the neutrinos do interact however, their properties, including flavor and energy and momentum, can be determined based on the products of their interaction. When a neutrino from the beam interacts with an argon nucleus it creates one

or more charged particles, ranging in number and type, depending on the properties of the neutrino. These particles pass through the liquid argon, ionizing argon atoms along their path. Electrons excited from the argon atoms by this process are then drifted across the detector, by the electric field, to the collection and induction planes, by which they are registered.

When a drifted electron comes close to a wire in either of the induction planes, which are held at a negative bias voltage, it curves around and past the wire, see Fig. 6 (7). The passing of this electron induces a small current pulse in the induction wire, proportional to the energy of the electron. After passing through the induction planes the electron is then collected on one of the collection plane wires, which are set with a positive bias voltage in order to attract the electrons. This collection of an electron also results in a current pulse proportional to the electron's energy. The energy carried by every drifted electron is the same, constrained by the electron mass and drift velocity. However, when the ionization electrons along the path of the passing particle are drifted towards the wire planes they will arrive in clusters. The clusters of electrons create the current pulses in the wires. The larger the cluster of electrons the more energy was deposited by the passing particle, and the larger the current pulse registered by the wires.

Every pulse registered by a wire in any one of the three planes has its amplitude and timing information, in addition to wire number, recorded and stored as a single hit. Since a single electron passes through all three planes, there will be three hits used to reconstruct the origin of the electron within the detector in in three dimensions.
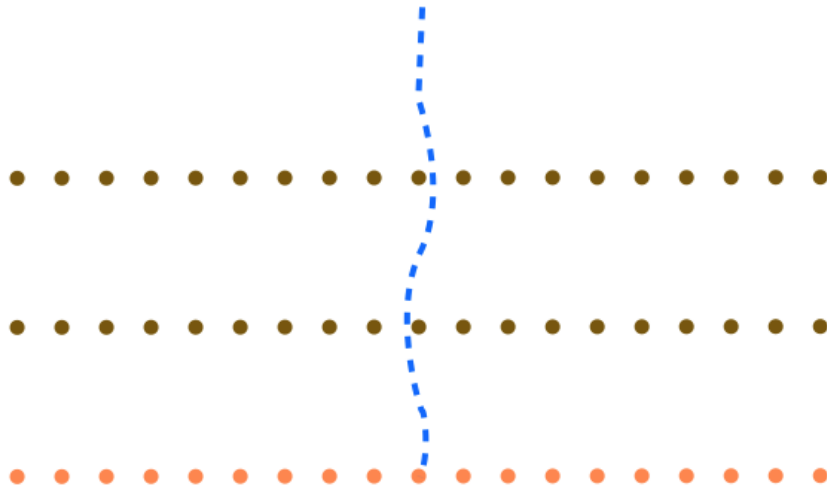
Fig. 6: The three sets of dotted lines represent the two induction planes, above, and the collection plane, bottom. A drifted cluster of electrons, represented by the dashed line, will bend around the two wires in the two induction planes, inducing a small current pulse. The electrons are then collected on one of the wires in the collection plane, also creating a current pulse. Each pulse is associated with a time and recorded as a single hit.

1.4 Reconstruction

Every hit defines a location within the detector in two dimensions. The wire

number gives the position of the hit in Z, though the wire numbers of hits from the

induction planes will be skewed due to the angling of the those wires. The timing of the

hit then gives the depth in the detector. This is the X dimension, with zero measured from

the center of the detector. In order to determine how deep in the detector the ionization

occurred from the timing information, two additional pieces of information are needed.

The first is the time at which the ionization occurred. Comparing this to the time at which

the hit was recorded gives the drift time of the cluster of electrons from the point of

origin to the wire planes. In order to determine this timing information the experiment

uses an array of photomultiplier tubes (PMTs). One of the advantages of liquid argon as a

detection medium is that it scintillates when there is an energy deposition. In other words:

when an interaction occurs within the liquid argon, for instance a neutrino interacting

with an argon atom, there will be a flash of light inside the detector. The PMT detects this

13

flash of light and the timing on the flash gives a start time for an event. The second piece of information needed is the electron drift velocity in liquid argon. When the electrons are created they are quickly accelerated to their drift (terminal) velocity, by the uniform electric field across the detector. Relating the time the hit took to drift across the detector to its drift velocity gives a reconstructed position of the hit's point of origin in X.

Based on the above reconstruction, every hit can be plotted in either XU, XV, or XY, depending on whether the hit was recorded by the induction or collection planes. If all hits for an event are plotted in their respective planes, we can then get a sense for what the particle tracks passing through the detector looked like from above the detector (oriented down a wire plane), see Fig. 7. Often, to save time in reconstruction these plots are not made in units of distance but rather are plotted as wire number vs. time counts. Rather than measuring time in seconds, the time counts are counted in TDC ticks, ~ 2 nanoseconds in length.

The the location of the electron in Y is then determined based on the geometry of the wires, where Y is measured from the bottom of the cage, to the top, with an origin in the middle of the detector.Wires the registering hits at the the same time are compared and points at which three wires intersect define the location of the electron in Z and Y, see Fig. 8. Having three, rather than simply two planes of wires allows more accurate reconstruction.
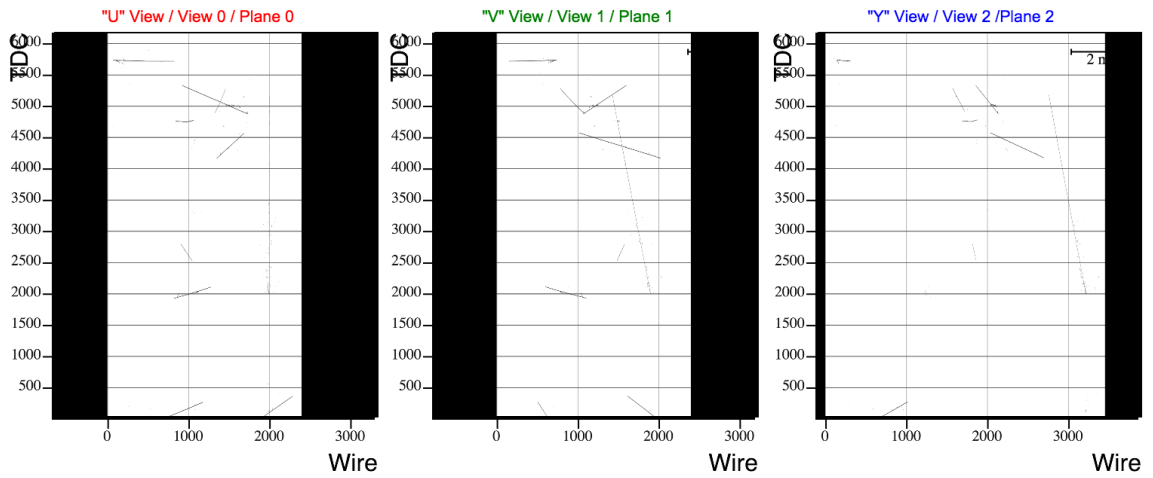
Fig 7: This shows all hits for an event plotted in tdc count vs. wire number for the three wire planes. In this case there are nine particle tracks, with each appearing at different orientation in each window

Fig. 8: Illustration of the unique identification of two two-dimensional hits, reconstructed in the YZ plane (circled). Wires which registered hits at the same time are shown in bold. A single point where one wire from each of the planes meets, identifies a single electron reconstructed in two dimensions.

15

2. Methodology

With the reconstruction understood the next concern is understanding the way in which data is recorded. When the signal is collected inside the detector, it is initially registered by the cold electronics, that is, the electronics within th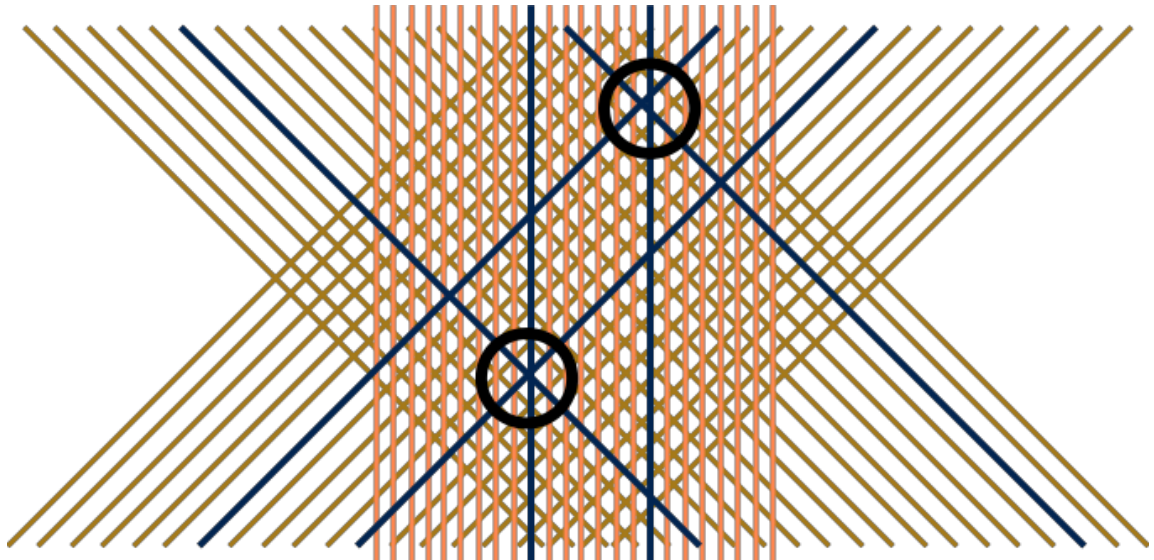e cryostat which need to be kept at liquid argon temperatures, roughly 90K (7). The signal is then transferred out of the cryostat to the warm electronics, where it is read out and recorded. Hit signals are recorded by analog to digital converters (ADC), which store information in uncalibrated units, called ADC units. Translating these ADC energies to usable data requires an understanding of how the recorded energies scale into standard usable units, i.e. electron volts (eV). In order to determine this scaling factor a "standard candle" is needed for comparison. For this study, Michel electron events were used as the "standard candle" for calibration. Michel electron is the name used to refer to electrons resulting from muon decay. These electrons are highly practical for calibration. Not only do they have a well understood energy spectrum, but they will also have a large presence in the detector, even before the experiment begins collecting beam data.

2.1 Muon Decay and Michel Electrons

Despite its location six stories below ground, the detector is still extremely close to the surface of the earth. As such, it is subject to a constant bombardment of particles, the largest contributor being cosmic rays, particles originating from space which interact with the earth's atmosphere. Upon entry, cosmic rays create a particle shower, a chain of particle interactions/decays, each successively producing more particles, see Fig. 9.
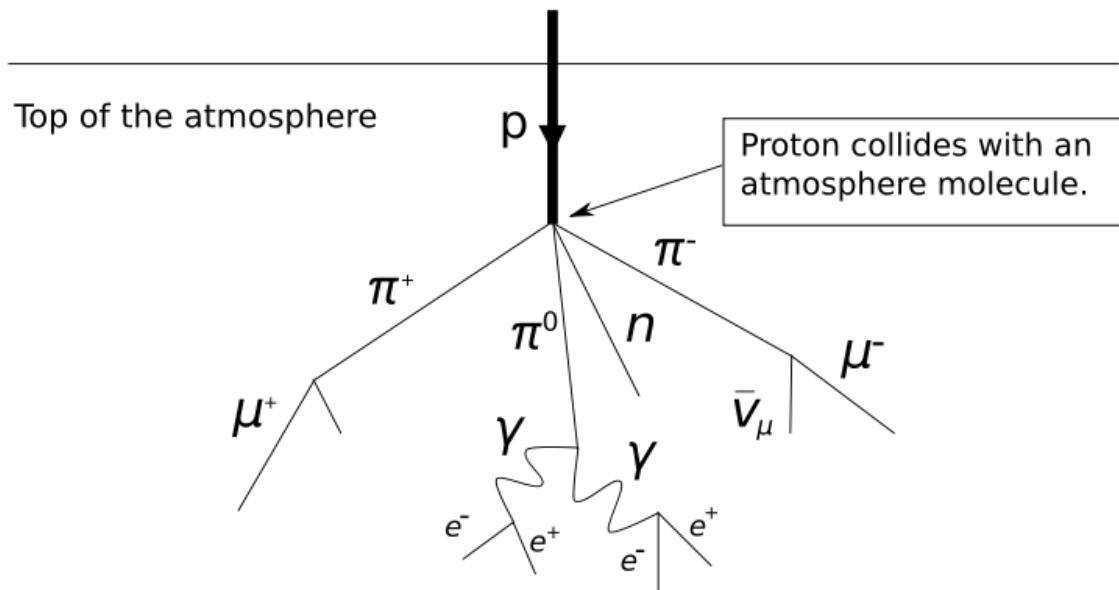
Fig. 9: Diagram of cosmic rays striking the upper atmosphere in a shower of particles. The muons of interest to the study can be seen on the far left and far right of the diagram

One of the main products of these cosmic ray showers that will make it into the detector are muons, which are leptons very similar to electrons, though approximately 500 times as massive. While muons have a half-life of only a couple microseconds, they are created traveling at relativistic speeds, so their time is dilated such that most make it to the earth's surface before slowing down and decaying. As such, muons will continuously be passing through the detector, with approximately 1% of them stopping and decaying within the fiducial volume of the detector. When muons decay, they have a characteristic, dominant decay mode in which they decay into an electron (e^-), a muon-neutrino (υ_μ), and an anti-electron-neutrino ($\overline{\upsilon_e}$); both this decay mode, and the decay of the anti-muon (μ^+) are given by Eq. 1 & 2, respectively. The electrons and anti-electrons (positrons) created in this decay are known as Michel electrons, for Louis

Michel who studied this decay and the energy distribution of the resultant electrons. (6) It

should be noted that in real data the ratio of these decays is not one-to-one. The way in

which each of these reactions occur in matter is also not the same. In the case of the μ^-,

the muon is often captured before decay, getting absorbed by an argon nucleus. These

captures will pose problems to the calibration process as their characteristic appearance is

also that of a stopped muon track. However, rather than a Michel electron at the end of

the track, it will have low energy photon activity resulting from the capture.

$$\mu^- \rightarrow e^- + \overline{\upsilon_e} + \upsilon_u \qquad\qquad (1)$$

$$\mu^+ \rightarrow e^+ + \upsilon_e + \overline{\upsilon_\mu} \qquad\qquad (2)$$

In 1949, Louis Michel experimentally determined the energy spectrum of

electrons created during muon decay, see Fig. 10(6). As can be seen from the Michel

spectrum, there is a half-bell distribution for the energies of electrons seen coming from

muon decays, with a sharp cut-off at approximately 53MeV. Knowing the energy

spectrum of electrons resulting from this form of decay, provides a way of calibrating the

detector by comparison with the spectrum of Michel electrons measured from muons

stopping in the detector. Measurement of the spectrum inside the detector would provide

a direct comparison between the ADC energy in which detector events are recorded and

SI units.

The added benefit of using the Michel spectrum as the standard candle for

calibration is that observing muon decays does not require the beam to be on. This has

two advantages. The first is that the detector will begin taking cosmic data before taking

beam data, so preliminary calibrations can be run on early data in order to provide results

before the experiment starts taking beam data. The second advantage is that the calibration process can run on data taken during times when the beam is off. This will significantly reduce the amount of background noise in any files being analyzed, as the interactions from the beam will only obscure the characteristic interactions being searched for.
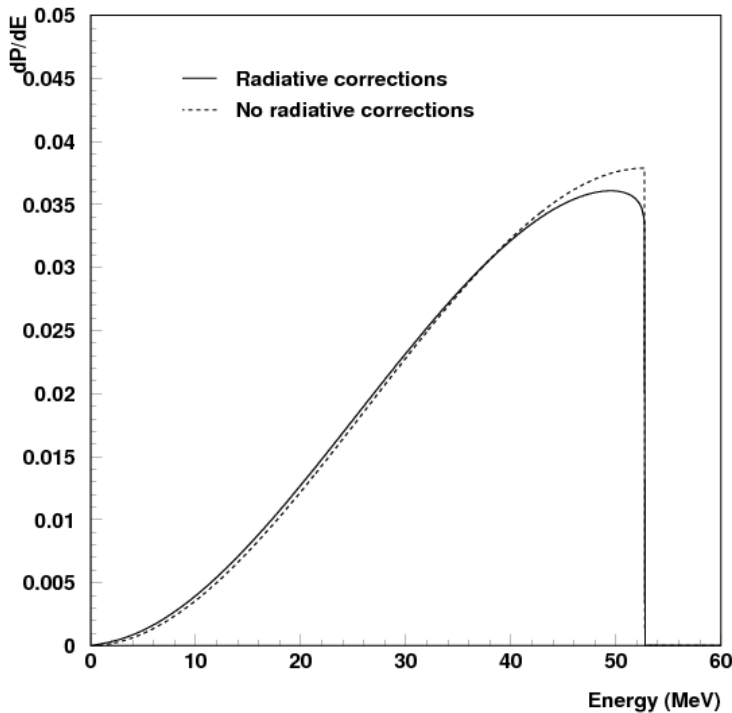

Fig. 10: The Michel electron energy spectrum as measured by Louis Michel in 1949. The half bell shape with the steep drop-off was the characteristic shape that was expected in the measurement of the spectrum within the detector, perhaps with rounding due to artificial lowered or raised candidate energies. (6)

2.2 Generation of Monte Carlo Data

Both to simplify the start of the project, and due to the fact that the experiment had not yet been placed into the ground by the beginning of the project, Monte Carlo data was used to begin development of the calibration program. Monte Carlo data is randomly generated data that is probabilistically accurate, and can be run to precisely simulate data as collected by the detector, or simulate simplified scenarios. The software designed for this experiment, known as LArSoft (Liquid Argon Software), provides a means of

generating Monte Carlo data for events inside the MicroBooNE detector. In addition to accurately simulating events within the detector, by nature of being generated data, the truth information for the events is also contained within the files. Truth information is simply a record of what was simulated for a particular Monte Carlo event. This means that for any data pulled by my calibration program, the results can be checked by a comparison with the truth data. However, truth checks were not placed in until later in development, and initial results and analyses were kept blind. The blind and truth analyses were performed during each stage of the project, which was seperated into three parts: analysis of generated single-muon events; analysis of generated multiple-muon events/cosmic events; and analysis of detector data.

2.3 Analysis of Generated Single-Muon Events

In order to ease the initial development of the program that would eventually be used to extract information from detector data, a number single-muon event Monte Carlo files were generated. These files simulated low-energy muons (~500 MeV) "fired" from a plane above the detector, isotropic in 2π. As this was meant to be a simplified simulation of real data, only 20-40% of the muons stopped in the fiducial volume of detector, while some passed through or missed entirely.

The ultimate goal of the project was to make the most robust method for Michel electron identification as possible which could be performed after only the simplest reconstruction of data had taken place. The process of analyzing the single-muon event files provided useful information on the pitfalls of trying to identify Michel electron candidates, even in a low noise setting.

The first level of reconstruction necessary for my process to work is the reconstruction of tracks. There are several trackers that have been developed for MicroBooNE, which run different mathematical algorithms on the hits to reconstruct particle tracks. Roughly speaking, a tracker loops through all hits within a single event, and runs some amount of reconstruction on them in order to associate hits that appear to fall along a single path. The amount of hit reconstruction required in order to reconstruct a track varies depending on the algorithms used, and the desired levels of efficiency and robustness. The Monte Carlo data generated for this project used two different trackers: trackkalsps and trackkalmanhit. The trackkalsps tracker reconstructs event tracks based on spacepoints, whereas the trackkalmanhit tracker reconstructs tracks based on a kalman filter. I began my analysis using a the trackkalsps tracker which provided insight on the pitfalls of a faulty, or overly simple tracker.

The method for extracting Michel electron data used in this project requires a functional track reconstruction. Identify candidate Michel electrons involves finding a reconstructed track and looking in a region centered around the end of that track for hits. Muons that decay into Michel electrons will have a characteristic chain of hits close to the end of their tracks, resulting from the Michel electron produced in its decay. Since Michel electrons result from a decay at the end of the track it is assumed that the activity at the end of a track is due to a Michel electron. Therefore summing up the energy of the hits in this region provides the total energy of the Michel electron. The size of the selection region was varied over several iterations, based on the distance a Michel electron would travel before depositing all its energy, roughly 20cm liquid argon. (2) It

proved necessary to find methods to veto hits coming from things other than Michel electrons, such as stray gamma rays or other particle tracks passing near the end of the track being investigated, the second of which was not an issue for the single-muon files.

However, the trackkalsps tracker incompletely reconstructed tracks. When reconstructing a particle track in the detector, only a portion of the hits along a track would actually be associated with the track. Fig. 11 has three plots showing an example of this problem for a single reconstructed track. The first plot shows a single-muon event, with a long muon track passing through the detector and decaying into a Michel electron, which forms a shorter track at the end. The middle plot shows all hits that have been associated with the muon track, labeled as "on-track" hits. The problem can be seen in the third plot, which shows hits that have not been associated a track, labeled as "off-track" hits. As can be seen in this plot, a large number of hits that fall along the muon track, where not associated with the track. This presents a large problem for the Michel electron selection process. In order to select candidate Michel electrons, circular regions are drawn around the end of the tracks in the detector. If there are hits around the end of the track, the energy of all the hits in that region is summed, and that event is taken as a Michel electron candidate. However, if a large number of hits from the muon track are left behind, this will artificially inflate the energy within the selection region, either distorting the energy of the Michel electron or creating false candidates.
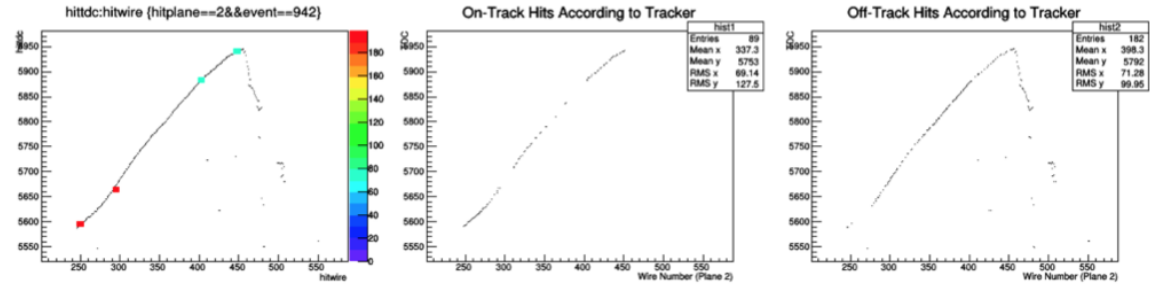
Fig. 11: Three plots of hit TDC count vs. wire number from the collection plane (plane 2), for all the hits in one single-muon event. These plots reconstruct tracks in the the XZ plane of the detector. In this case a long muon track can be seen decaying into a small michel electron track. The left image shows all event hits, with vertices and ends drawn in (here the track was broken into two segments). By comparison of the middle plot and right plots, which shows those hits that have and have not been associated to a tracks, respectively, it can be seen that not all hits from the muon have not been associated to the track.

As such it was necessary to develop a means of re-associating hits with tracks where appropriate. In order to do this, the vertex and end of the tracks were pulled from the reconstructed event file. These two reconstructed points were then used to define the corners of a square region in XZ plane of the detector, and a line was drawn between them. Points that fell within the box and within 10cm of the line were then associated with the track. The final shape of this vetoed region was an extend hexagon. Fig. 12 shows a cartoon illustration of the veto process. Ostensibly, this process rejects a quarter of the events in the sample used for this study, as Michel electrons are equally likely to be created heading in any direction relative to the muon track. If a Michel electron was created heading back in the direction of the original muon track, the hits from its track would then be selected as part of the track. However, without this cut, the measured energy would be artificially inflated as portions of the muon track might be left in the selection region. These facts, combined with the extremely high statistics available for the study, were taken as sufficient justification for this cut.
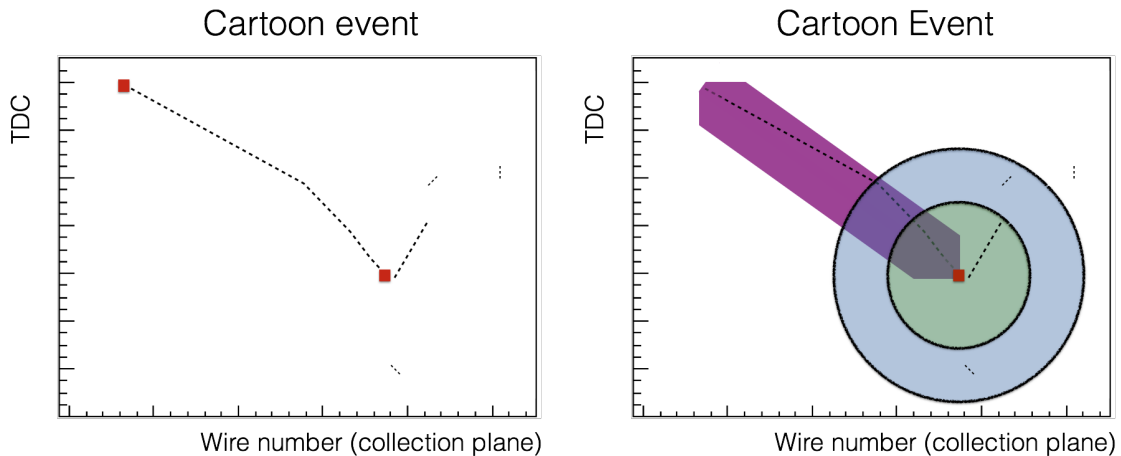
23

Fig. 12: An illustration of the track association process. In this cartoon event plots of TDC count vs. wire number for hits from one mock single-muon event are show. In the left plot a long muon track, with reconstructed track vertex and end point, can be seen decaying into a Michel electron track, with some small clusters of activity due to bremsstrahlung. In order to veto hits that fall along the path a cut was made of hits falling in the purple veto region around the muon track, non-vetoed hits within a circular region around the end of the track were then summed. With a secondary circular region used as a veto region.

Figs. 13 and 14, show example of the results of this track association process. Each has 6 plots, read from left to right and top to bottom, all in TDC counts vs. wire number from the collection plane. This effectively acts as a simple two dimensional event display, looking down on the detector. The first row of plots come from an event before the veto was applied. The second row of plots are from the same event after the veto has been applied. The first plot in each row show all the hits from an event. The second plot in each row show hits from the events that have been associated with a track. Ideally this plot would contain only hits due to the muon track. For the single-muon event files there would only be one muon and it was assumed that only the muon, not the Michel electron would be tracked. I will discuss this assumption further in the following section. The third plot shows hits that were not associated with a track, which would ideally contain only hits from the Michel electron, in addition to any background activity.
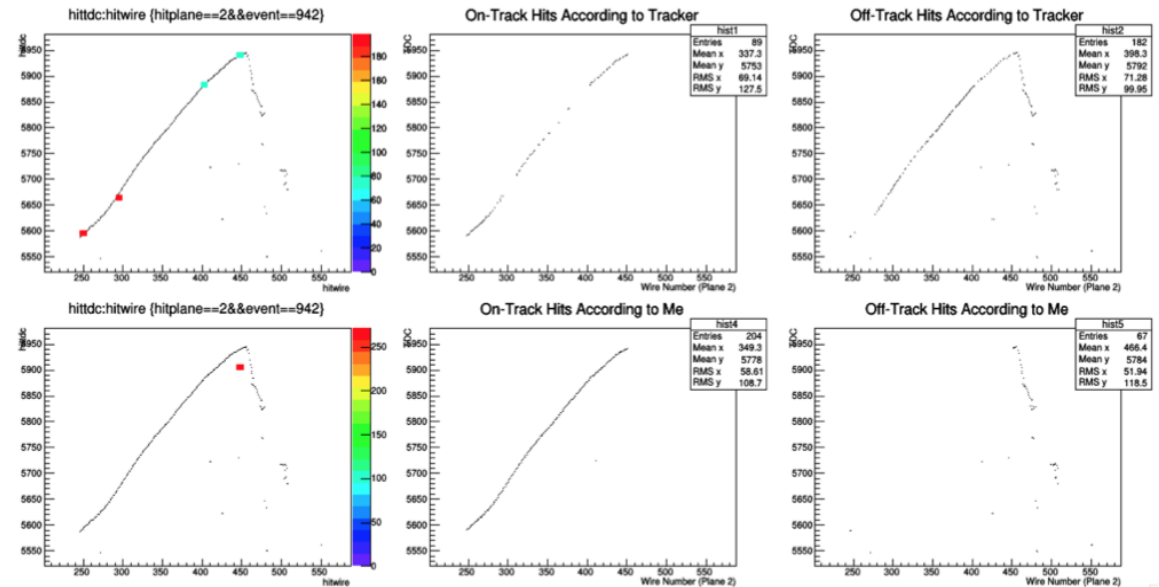
Fig. 13: This is an example of a successful application of the track association process on generated data. The top row shows all hits, hits associated with tracks, and hits not associated with tracks, using only the tracker. The bottom row shows the same data after the track association process illustrated in Fig.12 was applied.
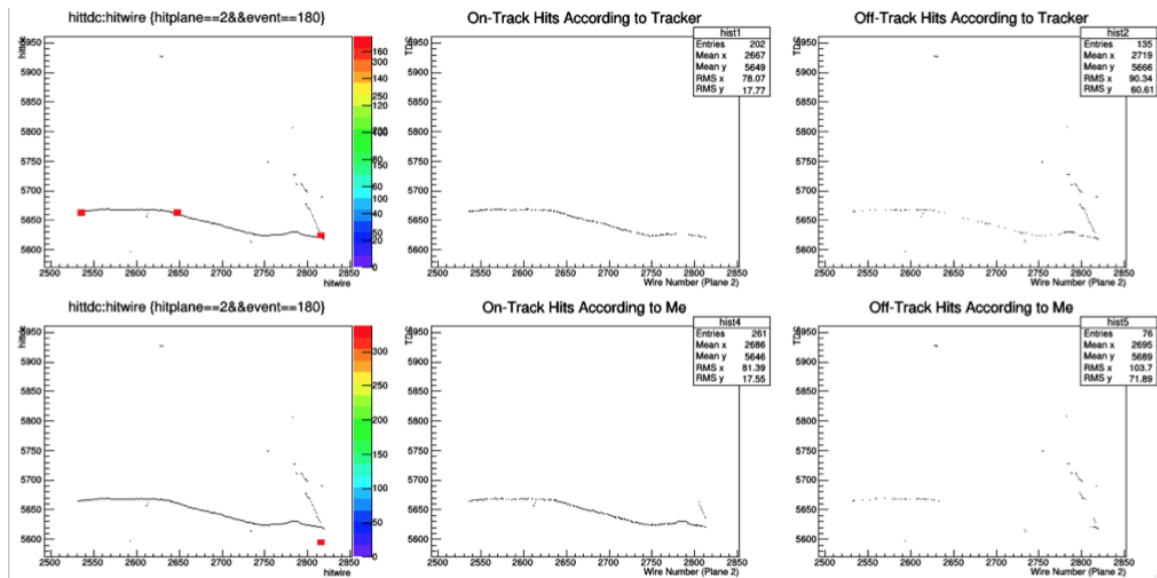

Fig. 14: This is an example illustrates two potential errors possible with the track association process. In this case, due to the shape of the track, the veto region did not fully select the hits from the track that were left behind by the tracker. In addition the track selection process selected a portion of the Michel electron track. Normally these two errors occur separately.

As can be seen from Fig. 14, the track association process does not fully compensate for the tracker errors in the case of particles that follow a curved path through the detector. The process can also occasionally select portions of the Michel electron track, which is only a problem if the track is not fully selected and leaves behind an artificially reduced number of hits to be summed up. However, this error was found to be the exception.

As part of process for selecting and summing hits around the end of the track, two other cuts were put in place to ease the transition to multi-muon event files. When selecting the hits within a certain radius of the end of the track an additional veto region was drawn around the selection region. Inside the selection region the number of hits was summed as well as the charge of all the hits in the region. Then a veto region outside the selection region was drawn and the number of hits and the sum of charges in that region were recorded. In identifying candidate Michel electrons, any candidates that had least half as much activity in the veto region was discarded. Three assumptions were made to justify this veto. Some tracks where no Michel electron was formed had low energy activity, comprised of a small number of hits, around the end of the track. Assuming this low energy activity was evenly distributed around the detector, just as much low energy activity would be seen in this veto region as the inside region, and these low-energy false-positives could then be vetoed. More importantly the veto region worked to veto events that had other tracks around their ends that might be mistaken for Michel electrons by the script. If another particle where to pass by the region at the end of the track under investigation, it was assumed it would pass through both the selection and the veto

regions, leaving a comparable amount of activity. Though this would mainly be helpful in

the transition to multiple-muon event files. The final justification behind the use of the

veto region was to discard candidates that selected only portions of the Michel track. In

finding the candidate energy of the Michels, several different size selection regions were

used. The average stopping distance for an electron of 50 MeV in liquid Argon is

approximately 20cm (2). Given that the the maximum energy of a Michel electron is ~ 53

MeV, this was taken as our assumed distance of travel. However, the two selection

regions drawn were 30cm and 50cm to act as padding around the end of the Michel track

to account for any Bremsstrahlung the electron underwent, emitting photons as it

decelerated, which would travel further in the detector. In fact, after comparison with

truth, it was found that the 50cm region tended to trend more linearly with the true

energy.

The trackkalsps tracker provided another warning about the reliability of the

trackers: occasionally the vertex and end of the track were mislabeled. Since the muons

in the simulation were coming in from a region above the detector, as any true muons

coming in from cosmic rays would be, the vertex of the track would be higher in the

detector than the end. However, occasionally the tracker reversed the two locations and

my script would search for hits near the mislabeled end of the track rather than the true

end of the track. As such, when identifying which end of the track to look around for

candidate Michel electrons, the program was rewritten to "trust" the tracker to locate the

vertex and end of the track, but selected which to look around based on height in the

detector rather than the labeling of the tracker.

An additional issue brought to light by the trackkalsps tracker was that the muon tracks were occasionally reconstructed in segments as multiple tracks. This can be seen in the first plots in Figs. 13 and 14, where track ends and vertices are plotted as colored points. While using data for single-muon events, which should only have a single muon track, this problem was overcome by stitching the tracks together. The process involved extending the veto region discussed in the previous section. Rather than using the vertex and end location for a single track, the vertex located highest in the detector and the end located deepest in the detector were used to form the veto region. However, this practice was ultimately abandoned when running analysis on files with multiple muons, as more than one track would be expected.
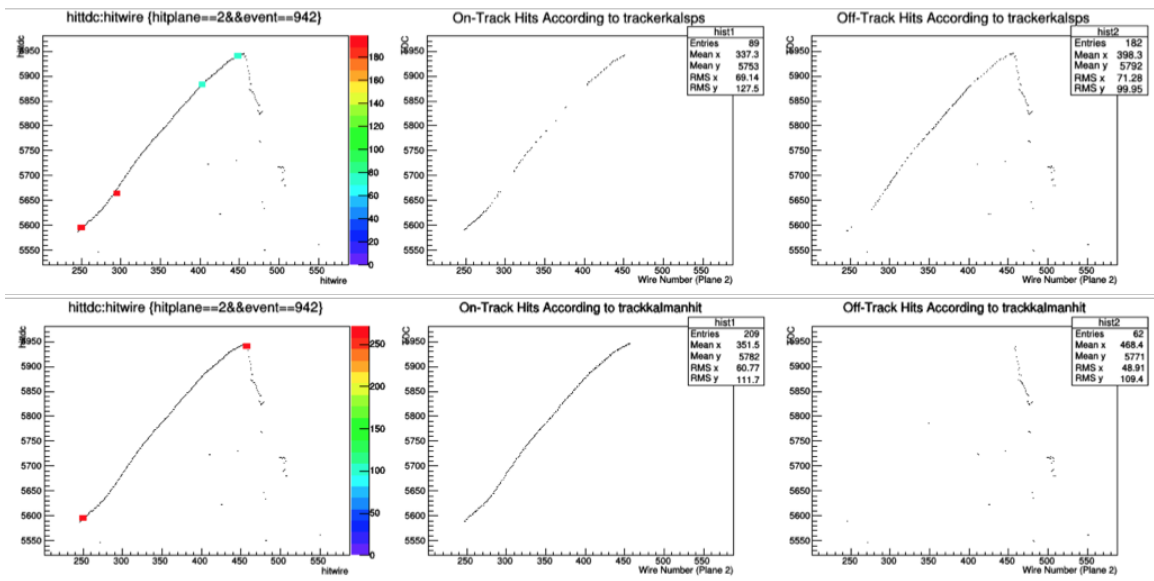

Fig. 15: This shows the comparison of a single event reconstructed using the trackkalsps tracker, top row, which is the same as Fig. 11, and the trackkalmanhit tracker, bottom row. Clearly the trackkalmanhit tracker more accurately associated hits with tracks and did not break the track into multiple segments.

Fortunately, the difficulty of the segmented tracks was overcome with a switch to the second tracker used in the reconstruction: trackkalmanhit. With this tracker the issue of segmented tracks was largely overcome, see Fig. 15. However, even with the new tracker, the track association process based on stitching the tracks together was left in the script for the single-muon analysis. By leaving in this cut, however, the experiment explicitly assumed, for this portion of the analysis, that any Michel electron event would not be tracked, which based on a hand-scanning of several hundred events was found to be true at least 90% of the time. When analyses were performed on multiple-muon event files it was determined that Michel electrons are almost never tracked.

With the improved tracker, the project saw a marked leap forward in accuracy. For each tracker a plot was made comparing the reconstructed Michel electron energy to the true energy, see the Fig. 16. In this case the true energy was determined by a hand-scan of the true data using the Argo, Dr. Nathaniel Tagg's online viewer software for the MicroBooNE experiment. The process of hand scanning events was instructive in learning the signature look of a Michel electron event. The hand scanning also provided an alternative should the script I wrote prove unable to pull out the Michel energies accurately, though such a process would be significantly more time-consuming and not allow for a contribution that might be incorporated into the experiment for continued use.

Fig. 16: The reconstructed vs. truth energy plots using the trackkalsps tracker, top, and the trackkalmanhit tracker, bottom. As can be seen the trackkalsps tracker seemed to leave behind a large number of excess hits, artificially increasing some of the candidate energies. However, both processes still suffer from a large number of low-Energy false-positives, and several, low energy candidtates.

Fig. 16 helped provide validity to the method of the study. When comparing the truth energy to the reconstructed energy a linear relation between the two would imply that the method of selection is accurately identifying Michel electrons. In the case of Fig. 16A, which is based on data from the trackkalsps tracker, there is only a slight linear trend, which, under investigation by hand-scanning, resulted from multiple factors. There

are several candidate Michel electrons where the previously discussed track-reassociation process improperly selected a portion of the Michel electron to be associated with the track. This artificially lowered the energies of several candidate energies, distorting the trend. There are also several candidates with very high energies, which resulted from segments of the muon track not being properly associated to the reconstructed track and then getting summed in as part of the reconstructed Michel electron energy. This also contributed to one of the problems seen in the trend, which can be seen along the bottom of the plot: a large number of candidate Michel electrons that do not correlate to a true Michel electron. If a track without a Michel electron near the end was improperly segmented or reassociated then there were occasionally large energies registered by the selection process, which counted the hits from the unassociated portion of the track as the energy of a Michel electron. Both the problem of unassociated portions of the track and the issue of improperly associating the Michel electron with the track can be seen in Fig. 14. There were also issues with low energy activity around the end of the detector which would be registered as a low energy candidate. This low energy activity was largely due to stray gamma rays in the detector, and will be discussed further in section 4.2.

With the switch to the trackalmanhit tracker the plot of truth vs. candidate energy became much more linear, as can be seen in Fig. 16B. The candidates with artificially high energies were reduced down to more accurate values, as segments of the track were no longer being left behind. This is evident not only in the more linear trend of the candidate vs. truth energies, but is also reflected in the fact that the false positive candidates are all low energy. However, the problem of portions of the Michel electron

track being associated to the muon track still remained, resulting in the deviations of a few low energy candidates from the linear trend. The problem of false positive candidates also remained, resulting, as previously stated, from low energy activity around the end of the track, unassociated with the Michel. The solutions to these problems were investigated as part of the move to multiple-muon files.

2.4 Analysis of Generated Multiple-Muon Events

For the multiple-muon analysis, a set of 100 one-hundred-event multiple-muon files were located in the the MicroBooNE Monte Carlo data-base. All these files were created using a more recent version of LArSoft than the single-muon files, and were designed to simulate muon events coming in from cosmic rays that stopped inside the detector. In order to speed up the script process, it was rewritten to pull needed information from hits and tracks into a more compact file containing the information relevant to my study. Each compact file contained two data structures, known as trees, one with information related to the muon tracks from all 100 events in the file, and one containing information about each of the hits in the file and their track associations. The tree of track information also contained truth information to perform an automated check of the selection process, and to generate a Michel distribution based on the truth data. The truth data was not directly associated with hits and therefore had to be associated as part of the scripts. This was done by comparing the true location of a Michel electron vertex with the end of a reconstructed track. However, as before, the Michel candidate selection process was kept blind from the truth.

Looping over every one of the tracks in the track tree allowed for an efficient search for Michel electrons based on the activity around the end of the track. A brief study was incorporated into one iteration to determine if Michel electrons were ever tracked. If so this would greatly improve the accuracy of the study as candidate selection would be a simple matter of looking for another track near the end of a candidate track and measuring its ADC energy. However, a study found that when looping through all 100 events in each of the 100 files, there were only two instances of tracks in the detector whose vertices or ends were within 30cm of one another. It should be noted that for the sake of convenience this portion of the study was conducted using reconstructed coordinates which were measured in centimeters, with the understanding that a later simplification might require a move back to wire number and TDC counts.

Running the same cuts vetoes as were used in the single muon study, a possible Michel energy distribution was plotted, still using the two selection regions with 30cm and 50 cm radii, see Fig. 17. It can be seen that application of the cuts based on the veto region around the selection region did serve to sharpen the peak. However, there is no clearly defined cut-off as expected for a Michel distribution. This lead to the considerations of what might cause such a smoothing out of the distribution. The first thing considered were those factors effecting the linearity of the truth vs. candidate energy from the single muon study. Vetoing a portion of the Michel track might have lead to shift of the spectrum towards lower energy. Selecting large portions of other tracks was also thought to be a contributing factor, as a large portion of track could pass through the selection region, registering more activity inside the selection region than in

the veto region, especially if there were already activity at the track's end due to a

Michel. It was also considered that some energy could be lost in the detector based on the

distance over which the cluster of electrons composing the hit would have had to drift in

order to reach the collection planes. The further back in the detector the hit originated, the

more likely it would have been to lose energy due to electrons in the cluster recombining.

However it was determined that there was no significant difference between the energies

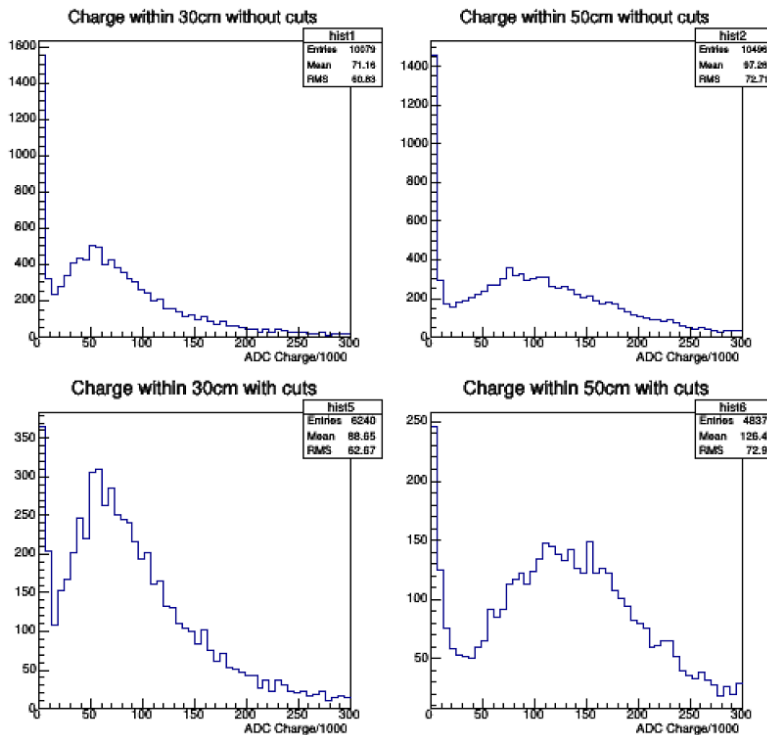seen in different locations in the detector.

Fig. 17: Plots of the Candidate Michel Energies. The top to plots show the plots of candidate energies for the two different selection regions, without any cuts based on the outer veto region. The bottom two plots show the same candidate energy plots, but with cuts applied based on activity in the veto regions. While the cuts do sharpen the peaks of the distributions, they do not produce the characteristic drop off of a Michel electron distribution.

In order to check that there was a Michel distribution to be measured, a plot was made of the truth distribution, see Fig. 18. The truth data shows clear resemblance to the Michel distribution shown in Fig. 10, with the characteristic rise to ~50 MeV before a sharp drop-off. However, a comparison of the truth and measured distributions presents a concerning discrepancy between the number of candidates and the number of true Michel electrons associated with tracks. It was found that the version of the trackkalmanhit used did not reconstruct with as high a degree of precision as the version used in the single-muon study, and split most tracks into two segments. As such, many candidates were in fact the result of the tracker reconstructing a track end halfway down a track, which triggered the candidate selection process, even though it was only measuring the energy of a portion of the track, not a Michel electron.
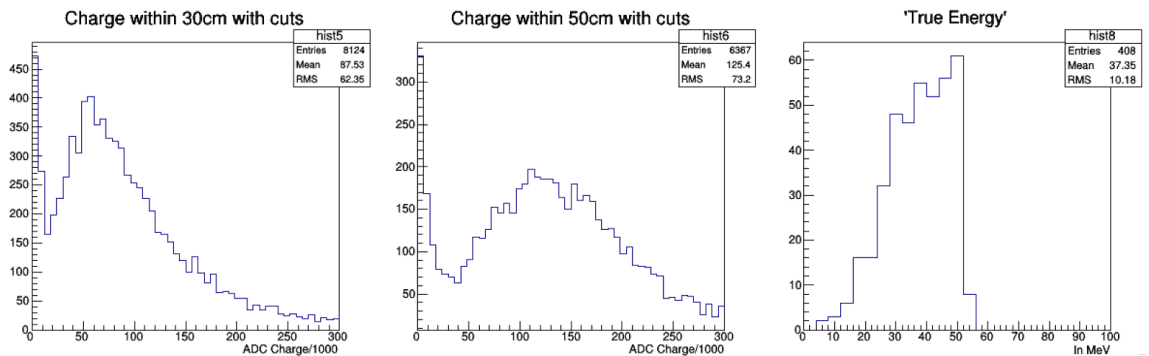

Fig. 18: Three plots, from left to right, showing the candidate energy distribution with a 30 cm selection region and a 50 cm selection region, and finally a truth distribution. While the truth distribution was intended to be used for comparison, it should be noted that the left two plots cannot be compared to the true energy plot, as the two contain highly discrepant numbers of entries. The measured plots contain 6000 to 8000 entries, corresponding to as many candidate Michel Electrons. However, for the region selected there are only 400 true events. The problem then is in the misidentification of candidate tracks.

The MicroBooNE detector has not yet begun to take data. However, once the detector is turned on and issues mentioned in the previous section have been overcome, the program will be ready to run on the detector data. To first order the particles passing through the detector, event with the beam on, will largely be cosmic rays. However, in addition to the few neutrino interactions that will occur within the detector on a daily basis, there will be a small number of other particles. The final step before the move to true detector data will be to run the program past a series of Monte Carlo files designed to simulate standard data recorded by the detector while the beam is turned off, and while the beam is turned on.

3. Results

3.1 Calibrations

The calibration factor for the detector was found at several stages of the experiment. For the single-muon portion of the study, using the data from the trackkalmanhit study, and a 50 cm selection region the calibration factor was found to be 770 ± 250 ADC/MeV. The large error on this value is predominantly due to the number of false positive candidates. There was also a calibration factor found for the data from the multiple-muon portion of the study, before the extent of the problems with the data were discovered, though the plots comparing the truth and candidate values are themselves indicative of a problem with the selection method as applied to the multiple-muon files, see Fig. 19. This figure shows a plot of the truth energy vs. reconstructed energy (note: the axes are the reverse of those seen in Fig. 16). In this case

there was not a clear linear trend, as there was in the case of the single-muon study. However to determine if the process was working on average, a slightly different analysis was performed. For each of the histograms of true energy vs. ADC energy, the histogram was profiled onto the Truth axis. That is, for each bin along the Truth axis, measured values of corresponding ADC energy were averaged. Performing this analysis yielded a linear trend. In other words, even though there was not a clear linear relation between reconstructed energy and truth energy, on average the higher the energy of the Michel electron being measured, the higher the candidate energy. This fit provided a loose calibration factor of 54 ± 8 ADC/MeV, which is in order with the calibration factor used by the most recent iteration of LArSoft for Monte Carlo data.

4.Discussion

4.1 Implications and Validity of the Study

At the time the single muon study was performed, the calibration factor found, 770 ± 250 ADC/MeV, was consistent with the factor used in generating Monte Carlo data. While the multiple-muon portion of the study did not translate as directly from the single muon portion of the studied as expected, the calibration factor of 54 ± 8 ADC/MeV is in agreement with the calibration factor used by the newest version of LArSoft. It is important to note that the single muon study and the multiple muon study were performed using data generated with two different versions of LArSoft, and thus have two distinctly different calibration factors.
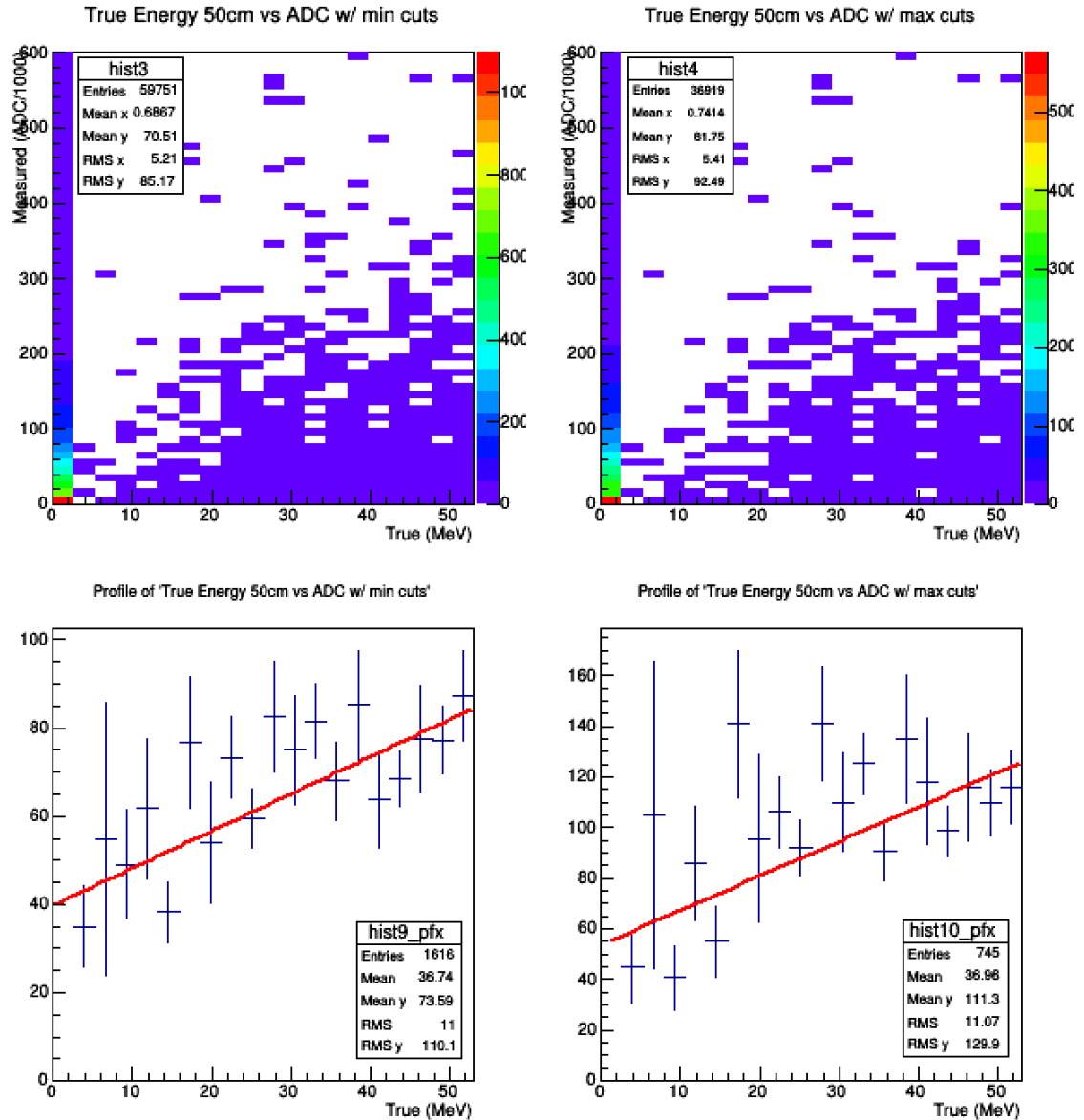
Fig. 19: This figure shows the truth data vs. reconstructed energy for the multiple-muon study. Top left shows all true energies plotted against the reconstructed energies they are associated with. The top right shows the plot for true electron energies plotted against all candidate events. This plot is dominated by false positives. Each of the top plots was profiled and fit to linear regression line, see bottom plots. While the first plot on the bottom does appear to be linear, it is, in fact distorted by the number of truth events for which there was a zero reconstructed energy. The bottom right plot is actually the fit used to provide the calibration constant. While the constant does not come from a linear relation of the truth to reconstructed data, it does show that for all measurements we get a pretty uniform value.

While this study was not able to produce a calibration factor with the degree of precision desired, it did not provide unreasonable data. The largest success of this study is a demonstration that the method, while not yet applied successfully to more complicated models, does in fact work. The linear trend from the single-muon study, seen in Fig. 16, shows that the method is not without merit. Even though the multiple-muon study did not produce the desired linear relation between true and ADC energy, it was found that, on average, the higher the true Michel electron energy, the higher the measured energy. However, more work will be required to carry this project forward to more complicated multiple-muon files.

4.2 Further Work

The future of this experiment will largely be determined by its ability to reconstruct the Michel spectrum accurately using the multiple-muon data. It has already been demonstrated that, with a functional tracker, finding a linear correspondence between truth and reconstructed data is possible. The next piece of further work for this project will involve investigating the functionality of the preferred tracker, as applies to the new data. Currently it is not reconstructing tracks in segments, and otherwise not functioning as well as the version used in the single-muon study.

The biggest concern is getting the reconstructed and truth energy to relate to each other as linearly as possible. However, even if the ultimate analysis should prove inconclusive, there is the possibility of using the data collection process of this experiment to determine the energy loss of electrons passing through the liquid argon. As stated, there is no energy loss modeled in the Monte Carlo. However the process used in

this experiment could be altered in order to provide such a calibration. Performing this study would not only be of significant interest to the experiment, as analysis depends on reconstruction of drifted electrons, but would also help provide a correction to the reconstructed energies measured as part of this experiment, and thus present a natural extension to the project.

Before carrying the project forward with further investigation into the multiple-muon files, there are other cuts to investigate in the single-muon files, though they will be equally applicable to both. As mentioned, Fig. 16B, while significantly more linear than the Fig. 16A, still has a large excess of low-energy false-positives. These false positives were largely due to low-energy activity around the end of the tracks, see Fig. 20. This low energy activity can either be a part of the detector background, or a result of a muon capture, a muon being absorbed by an atom before it decays, see Fig. 20.

A "nearest neighbors" veto process could be used to account for this. The cut requires a number of hits (usually 3-8) in the selection region to have a minimum number of hits within an ~8mm radius of themselves before that selection would be listed as a candidate. This sort of process would be very useful in the case of a smattering of low-energy activity, like that seen in Fig. 20. However, in those instances where only a portion of the Michel electron track is left behind, it would not be quite as helpful, as the hits would still be in a line.
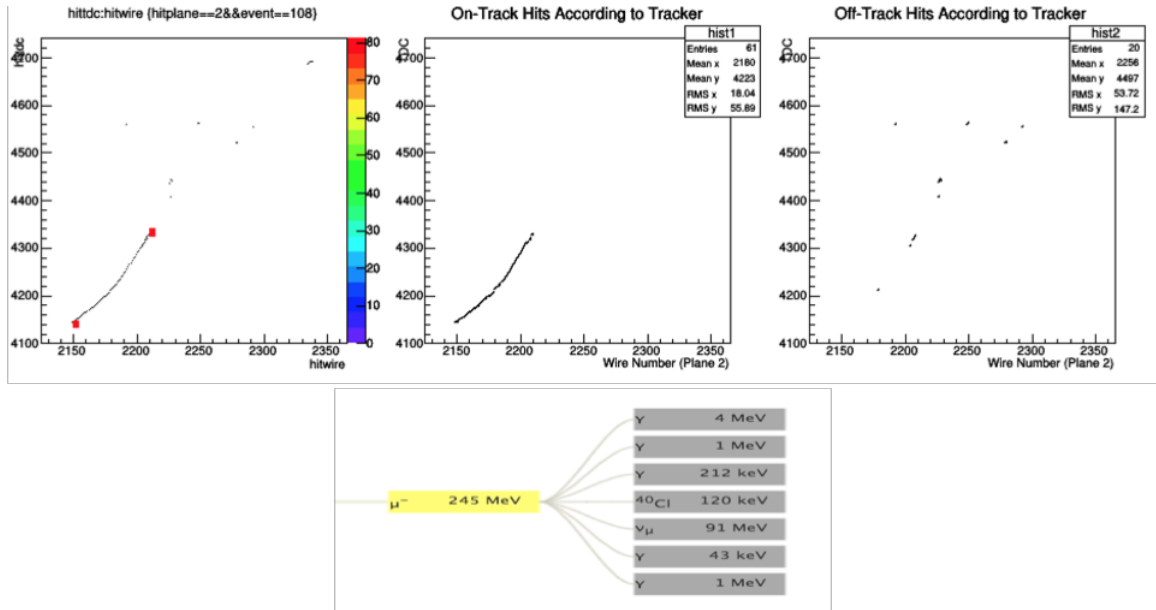
Fig. 20: While the track is almost fully selected in this event, and there is no Michel electron present, events like these were often registered by the program as candidate events for the low energy activity at the end of the track, and the portions of track that were left unselected. They formed the excess of low-energy false positives seen in Fig. 16B. In this example the truth data shows that this is not a true Michel electron event, even though it was selected as a candidate. Rather is a muon being captured by an argon atom before decay.

An alternate version of this veto, which would be useful both for false positive candidates and artificially increased Michel electron candidates, is an inertia tensor check. This would effectively give a sense of the shape of the hits being selected as a candidate electron. If the candidate is a good one it will be composed of a single track, and this will be reflected by the tensor, which will show the hits falling along a single line. Any candidate composed of spread out clusters of hits, such a Fig. 20, would be cut out due to their non-linear distribution. This would also cut out the artificially high Michel electron candidate as well, ones that are selecting a portion of another track in addition to the Michel, as the hits will fall into two lines, not a single line.

While the project had success in the early stages with single-muon files, the results did not translate directly into a multiple-muon setting, as hoped. This was due in

part to faulty track reconstruction, which left the tracks segmented, artificially inflating the number of candidates. However, there may also have been problems related to the way in which the truth information was associated with the reconstructed data. In addition to investigating these issues further, a return to the single-muon files may be necessary, in order to clear up some of the outstanding issues, rather than attempting to solve them in a multiple muon situation. While the study did not provide the results that were hoped, they have shown that this is a valid method, worth further investigation in simplified settings before moving on to more complicated settings.

6. References

1. Clairemont, Molly J. *Study of Positive Muon Decays in the MINERvA Detector*. 2012. Print.

2. "ESTAR : Stopping Power and Range Tables for Electrons." *estar: Stopping-Power and Range Tables for Electrons*. National Institute of Standards and Technology, n.d. Web. 27 Feb. 2015. <http://physics.nist.gov/cgi-bin/Star/e_table.pl>.

3. The ICARUS Collaboration. *Measurement of the Mu Decay Spectrum with the ICARUS Liquid Argon TPC*. 2003. Print.

4. *Long-Baseline Neutrino Experiment (LBNE) - Fact Sheet*. N.p.: n.p., 2013. http://lbne2-docdb.fnal.gov/cgi-bin/RetrieveFile?docid=6710;filename=DRAFT_ LBNE_Factsheet_4Pager_051413.pdf;version=4

5. Melnikov, Kirill. "Electron Spectrum in Muon Decay." Aug. 2005. Speech.

6. Michel, Louis. *Interaction between Four Half-Spin Particles and the Decay of the Mu-Meson*. 1949. Print.

7. The MicroBooNE Collaboration. *The MicroBooNE Technical Design Report*. 2012. Print.

8. MiniBooNE Collaboration. *The Neutrino Flux Predictions at MiniBooNE*. N.p.: n.p., 2009. Print.   http://arxiv.org/pdf/0806.1449v2.pdf